RSC Advances

PAPER

View Article Online
View Journal | View Issue

Cite this: *RSC Adv.*, 2020, **10**, 909

Using a visible light-triggered pH switch to activate nanozymes for antibacterial treatment†

Juqun Xi,[abc] Jingjing Zhang,[a] Xiaodong Qian,[d] Lanfang An[a] and Lei Fan *[e]

Received 10th November 2019
Accepted 23rd December 2019

DOI: 10.1039/c9ra09343e

rsc.li/rsc-advances

Here, we develop a visible light-triggered platform to activate the biomimetic activity of CuS nanoparticles by incorporating a photoacid generator. Under visible-light illumination, the remarkable pH decrease, caused by the intramolecular photoreaction of the photoacid generator, activates the peroxidase-like activity of the CuS nanoparticles. This visible light-triggered pH switch meets the antibacterial demands of peroxidase mimics perfectly in bacteria-infected wounds. Importantly, the built-in torches of mobile phones are able to replace the visible-light source to activate the peroxidase-mimicking activity of CuS nanoparticles to combat bacteria, which greatly promotes the utility and adaptability of this antibacterial platform.

Introduction

Nanozymes have aroused much interest due to their practical advantages over natural enzymes, including high stability, straightforward preparation, and low cost.[1] A growing number of nanomaterials have been found to exhibit enzyme mimetic activities, such as that of oxidase, peroxidase, superoxide dismutase, and catalase.[2] These activities of nanozymes have since been applied to bio-analysis,[3] disease diagnosis and therapy,[4] and environmental chemistry.[5] For example, the catalytic reaction of peroxidase, which can convert hydrogen peroxidase (H_2O_2) into highly toxic hydroxyl radicals ($^{\cdot}OH$), has been widely used to kill cancer cells and bacteria.[6] For instance, peroxidase mimics (such as Au,[7] Fe_3O_4,[8] and graphene[9]), with the assistance of H_2O_2, have been widely utilized to treat bacteria-infected wounds. However, similar to horseradish peroxidase (HRP), the activities of peroxidase mimics are pH dependent, with most being inactive at near neutral pH.[10] As for wound treatment, the pH of infected sites ranges from 6.5 to 8.5, with higher pH for more severe infections.[11] This feature easily decreases the antibacterial effects of peroxidase mimics. Therefore, understanding how to activate and maintain peroxidase-like (POD) activity of nanozymes in bacteria-infected wounds is highly desirable to promote the application of nanozymes in biomedicine.

To overcome this problem, we introduced a photoacid generator (PAG) to a nanozyme/H_2O_2 antibacterial system. PAGs, as photoinduced acid sources,[12] attract widely attention due to their wide applications in photolithography, polymerization, and stimuli-responsive systems.[13] Especially, PAGs possess the ability to induce proton dissociation under light irradiation, thus changing pH of an aqueous solution.[14] Protonated merocyanine (MEH) is reported to be a long-lived PAGs. As shown in Fig. S1,† under visible-light illumination, a proton is rapidly generated through the intramolecular photoreaction of MEH, resulting in a decrease in pH.[15] This unique physicochemical property meets the antibacterial demands of peroxidase mimics perfectly.

In this work, we synthesized albumin-stabilized copper sulfide nanoparticles (CuS NPs). CuS, known as a semiconductor, has received wide attention because of its potential application in electronic, optical and catalysis fields.[16] Besides the applications as a semiconductor, CuS, with low systemic toxicity, also shows great potential in biomedical fields, such as bio-molecular sensing, cancer therapy, and molecular imaging.[17] Here, we found that CuS exhibited obvious activity as an excellent peroxidase (POD) mimic. In particular, with the assistance of MEH and irradiation of visible light, the POD-like activity of the CuS NPs was activated in the wounds, thereby exerting a remarkable antibacterial effect and accelerating the wound-healing process. In addition, the release of Cu^{2+} from CuS mixed system containing MEH could also be triggered by visible-light irradiation, thus further enhancing the antibacterial effects. It was worth stressing that the built-in torches of mobile phones, including iPhone, HUAWEI, XIAOMI, and OPPO, were able to replace the visible-light source to activate

[a]*Institute of Translational Medicine, Department of Pharmacology, School of Medicine, Yangzhou University, Yangzhou, Jiangsu, 225001, China*

[b]*Jiangsu Key Laboratory of Integrated Traditional Chinese and Western Medicine for Prevention and Treatment of Senile Diseases, Yangzhou, Jiangsu, 225001, China*

[c]*Jiangsu Co-Innovation Center for Prevention and Control of Important Animal Infectious Diseases and Zoonoses, College of Veterinary Medicine, Yangzhou, 225009, Jiangsu, China*

[d]*Department of Cardiology, First Affiliated Hospital of Soochow University, Suzhou, 215006, Jiangsu, China*

[e]*School of Chemistry and Chemical Engineering, Yangzhou University, Yangzhou, 225002, Jiangsu, China. E-mail: fanlei@yzu.edu.cn*

† Electronic supplementary information (ESI) available. See DOI: 10.1039/c9ra09343e

the POD-like activity of the CuS NPs, which greatly promoted the utility and adaptability of our antibacterial platform in practical application.

Results and discussion

Herein, the CuS NPs were prepared by directly mixing $CuCl_2$ and Na_2S solution in the presence of bovine serum albumin (BSA) at 90 °C for 15 min.[18] BSA was utilized here to control the stability and size of the CuS NPs during synthesis.[19] A typical High Resolution Transmission Electron Microscope (HRTEM) image of the CuS NPs was shown in Fig. 1a. Based on statistical analysis (Fig. S2†), the average size of the CuS NPs was *ca.* 6 nm in diameter. Additionally, the dark field TEM image and the corresponding element mapping images of CuS NPs were shown in Fig. 1b–g. Besides the signals of Cu and S from CuS, we also observed the C, N, O signals from BSA, which indicated that BSA molecules coated uniformly in CuS NPs. Fig. 2a showed the powder X-ray diffraction (XRD) patterns of the CuS NPs, which were indexed to standard CuS (JCPDS No. 06-0464).[20] X-ray photoelectron spectroscopy (XPS) spectra (Fig. 2b and S3†) demonstrated the presence of Cu, S, C, O, and N elements in the CuS NPs. The C, N, and O peaks derived from BSA also indicated the successful coating of BSA on the surface of the CuS NPs. The Cu 2p peaks, due to Cu $2p_{3/2}$ and Cu $2p_{1/2}$, appeared at 932.12 and 952.08 eV (Fig. 2c), respectively, corresponding to Cu(II).[21] Moreover, by comparing the TGA (thermogravimetric analysis) curves of BSA and BSA coated CuS (BSA–CuS), the percentage of CuS in BSA–CuS nanocomposites was about 18% (w/w) (Fig. 2d). Over all, these results illustrated the successful synthesis of the BSA coated CuS NPs.

To achieve visible light-activated POD-like activity of the CuS NPs, a photoacid generator plays an important role. The working principle was illustrated in Fig. 3a. Firstly, MEH was synthesized according to previous research and its chemical structure was confirmed by ^{1}H Nuclear Magnetic Resonance (^{1}H NMR) spectroscopy,[22] as shown in Fig. S4.† The UV-Vis spectra of MEH (Fig. 3b) before illumination showed a characteristic

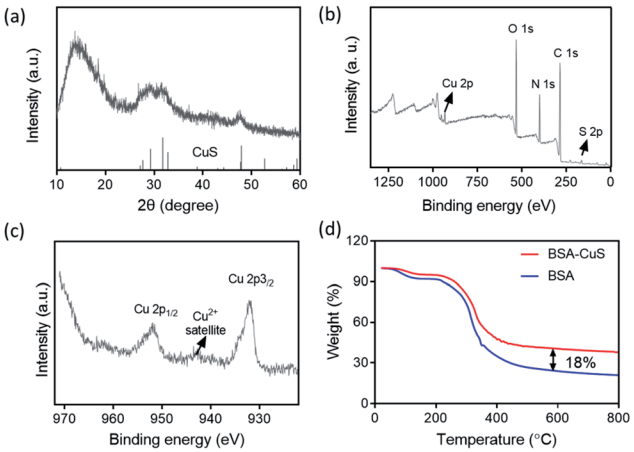

Fig. 2 (a) XRD pattern of the CuS NPs. (b) XPS spectrum of the CuS NPs. (c) Cu 2p high-resolution XPS spectrum of CuS NPs. (d) TGA curves of BSA and BSA coated CuS NPs.

absorption peak at 424 nm. Upon visible-light irradiation, the absorbance of MEH decreased quickly by 75.5% in 20 s (Fig. 3c), indicating its rapid photoreaction. Moreover, the initial pH of the MEH solution was about 5.8. When the MEH solution was irradiated with visible light, the color of the solution changed from yellow to colorless (Fig. 3d, inset), and the pH decreased to 4.1 within 60 s (Fig. 3d). Moreover, in the dark, the absorbance of MEH slowly returned within 10 min (Fig. S5a and b†), and synchronously, the pH increased gradually and reverted to 5.8 (Fig. S5c†). It was worth stressing that the color fading of MEH (from yellow to colorless) was also triggered by illumination from the built-in torches of mobile phones. As shown in Fig. S6,† the built-in torches of different mobile phones, including iPhone, HUAWEI, XIAOMI, and OPPO, also caused the rapid decrease of MEH absorbance at 424 nm in 30 s, indicating that the proton dissociation of MEH molecules could be triggered simply and conveniently with such devices. Furthermore, during the five on/off cycles of visible-light

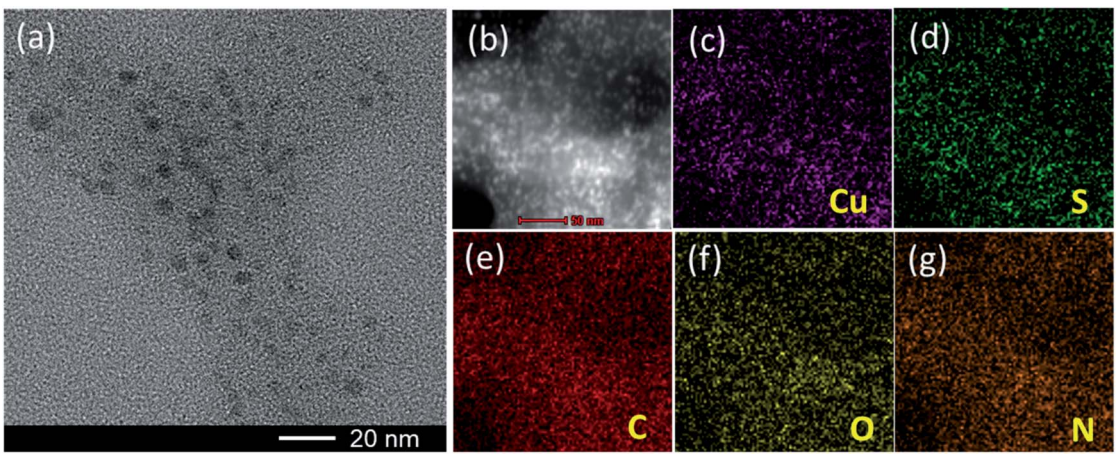

Fig. 1 (a) HRTEM image of the CuS NPs. (b) Dark-field TEM image of the CuS NPs. (c–g) TEM elemental mappings of Cu, S, C, O and N in the CuS NPs, respectively.

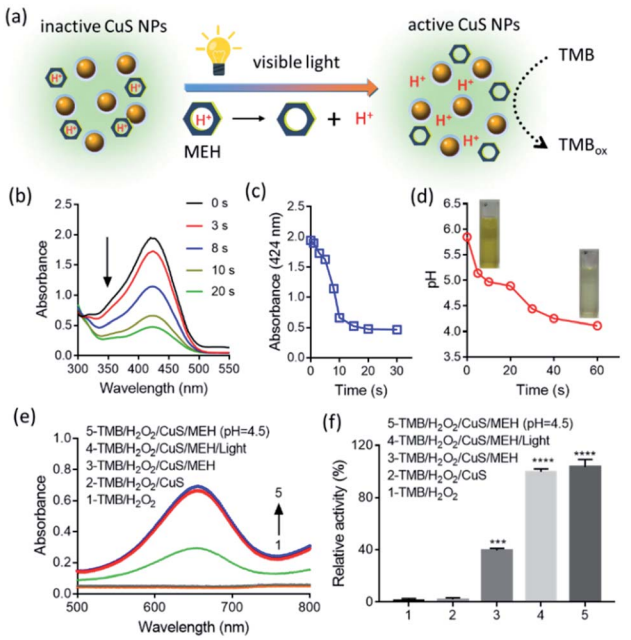

Fig. 3 (a) Schematic of visible light-activated POD-like activity of CuS NPs. (b) Time-dependent UV-Vis spectra of MEH solution under illumination. (c) Absorbance of MEH at 424 nm *vs.* time. (d) Time-dependent pH of MEH solution upon exposure of visible light. Insets were relevant photos. (e) Absorption spectra of TMB and (f) relative POD-like activity of CuS NPs under different conditions. Initial pH was 7.0 unless otherwise stated. [MEH] = 200 μM; [TMB] = 1.25 μM; [CuS] = 20 μg mL^{-1}; [H_2O_2] = 0.5 mM. Illumination conditions: λ = 350–780 nm, P = 37.5 mW cm^{-1}.

irradiation, the MEH solution maintained good proton dissociation ability (Fig. S7†), indicating that MEH was a stable, recyclable, and long-lived photoacid.

Next, we evaluated the POD-like activity of the CuS NPs. 3,3′,5,5′-tetramethylbenzidine (TMB) was used as a substrate to yield a TMB$_{ox}$ product during catalytic reaction. As shown in Fig. S8,† the CuS NPs efficiently catalyzed the oxidation of TMB in the presence of H_2O_2 to produce TMB$_{ox}$ with a characteristic absorption peak at 652 nm. In contrast, the reaction rarely occurred in the absence of H_2O_2 or CuS NPs, confirming that the intrinsic POD-like activity was a typical property of the CuS NPs. Analyzing the curves using the Michaelis–Menten equation, we detected the maximum initial velocity (V_{max}) and Michaelis–Menten constant (K_m), with results shown in Fig. S9 and Table S1.† Similar to HRP, the catalytic activity of the CuS NPs was dependent on pH and temperature (Fig. S10†).[23] More precisely, the CuS NPs showed the strongest POD-like activity at pH 4.5. With the increase of pH, the catalytic activity of the CuS NPs decreased gradually. At pH 7.0, the relative POD-like activity of CuS NPs was only about 20% of the maximum activity. This result demonstrated that the CuS NPs hold the pH-dependent POD-like activity, and this activity easily inactivated at near neutral pH.

Then, we investigated whether visible light could activate the POD-like activity of the CuS NPs in the presence of MEH at neutral pH. As shown in Fig. 3e, at pH 7.0, no distinct absorption peak of TMB$_{ox}$ was observed at 652 nm in the TMB/H_2O_2 and TMB/H_2O_2/CuS groups, suggesting that the POD-like activity of the CuS NPs was inactive. After adding MEH to the TMB/H_2O_2/CuS system, a weak absorption peak could be detected at 652 nm. This partial activity recovery of the CuS NPs was due to the MEH solution itself being weakly acidic (pH 5.8). Importantly, after visible-light illumination, the TMB$_{ox}$ absorption value was further promoted to its maximum value obtained at pH 4.5. The relative activity under different conditions, as shown in Fig. 3f, indicated that the POD-like activity of the CuS NPs nearly returned to its maximum vitality upon visible-light exposure. Thus, the pH decrease induced by irradiation of photosensitive MEH almost entirely activated the POD-like activity of the CuS NPs.

Subsequently, we tested the antibacterial activity of CuS NPs/H_2O_2 system under different pH conditions. As shown in Fig. S11,† under weakly acidic conditions (pH = 4.5), the combination of CuS/H_2O_2 was effective at suppressing the growth of both *Staphylococcus aureus* (*S. aureus*) and *Escherichia coli* (*E. coli*). At near neutral pH (7.0), however, bacterial growth was not observably inhibited. We also noted that the CuS NPs without H_2O_2 at pH 4.5 partially inhibited the growth of *E. coli*. This antibacterial activity could be attributed to the release of Cu^{2+} ions from the CuS NPs under weakly acidic conditions (Fig. S12†), and Cu^{2+} ions were proved to process the antibacterial ability.[24] Just as shown in Fig. S13,† the Cu^{2+} derived from $CuCl_2$ exhibited relatively strong antibacterial activity against *E. coli,* but less effective activity against *S. aureus*. Overall, our results indicated that the antibacterial nature of the CuS NPs (based on their POD-like activity) was pH dependent and was only activated under acidic conditions.

Regarding the pH dependence of antibacterial ability, we expected that visible-light illumination was able to activate the antibacterial activity of the CuS NPs in the presence of a photoacid. Exclusion experiments, including irradiation time and concentration of MEH, were first carried out. As shown in Fig. S14,† with the increase of irradiation time (0–15 min) or MEH concentration (0–500 μM), the bacterial viability (*S. aureus* and *E. coli*) was well maintained, indicating that exposure to visible light or MEH alone slightly affected bacterial viability. In the following tests, we fixed the concentration of MEH at 500 μM and the powder density at 375 mW cm^{-1} for 15 min. As shown in Fig. 4a for *E. coli*, the CuS/MEH/light and CuS/H_2O_2/MEH/light groups showed significant differences to the control group. No distinct antibacterial activity was observed for the other groups at pH 7.0. Moreover, the CuS/H_2O_2/MEH/light group was able to kill *E. coli* with −3.6 log-reduction, demonstrating a 630-fold increase in antibacterial activity compared with the CuS/MEH/light group. Similar antibacterial effects were shown towards *S. aureus* (Fig. 4b).

To further investigate the antibacterial mechanism of the CuS NPs, we assessed oxidative state in the bacterial strains. As reported,[24,25] the antibacterial activity of Cu^{2+} was mainly resulted from the lipid peroxidation. Here, the lipid peroxidation was tested using a malondialdehyde (MDA) assay. Taking *E. coli* as an example, compared with the control, MDA levels increased by four-fold and two-fold in the CuS/H_2O_2/

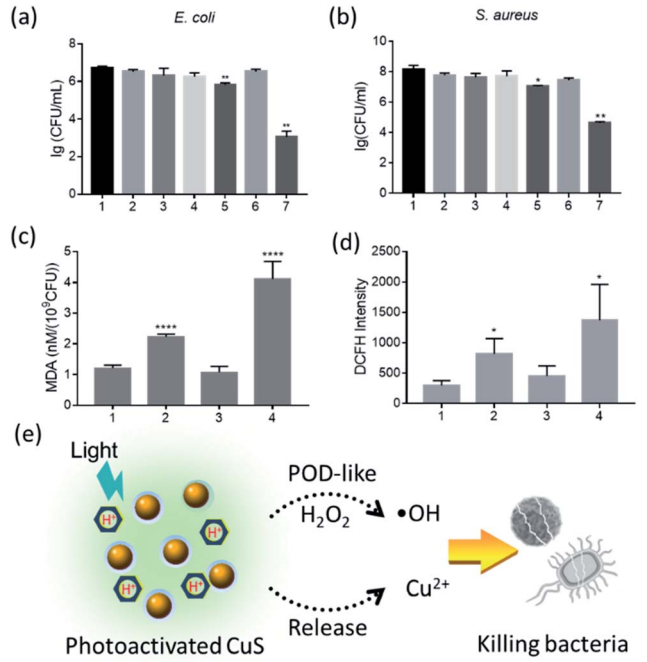

Fig. 4 (a and b) Antibacterial activity of CuS NPs against *E. coli* and *S. aureus* under different conditions. (1) Control; (2) MEH/light; (3) H_2O_2; (4) CuS/MEH; (5) CuS/MEH/light; (6) CuS/H_2O_2/MEH; (7) CuS/H_2O_2/MEH/light. Lipid peroxidation (c) and ROS levels (d) of bacteria under with different treatments. (1) Control; (2) CuS/MEH/light; (3) H_2O_2; (4) CuS/H_2O_2/MEH/light. (e) Schematic of visible light-activated CuS NPs to combat bacteria. Initial pH is 7.0 unless otherwise stated. [MEH] = 500 μM; [CuS] = 500 μg mL^{-1}; concentration of H_2O_2 was fixed at 1.0 mM and 10.0 mM for *E. coli* and *S. aureus*, respectively. Illumination conditions: λ = 350–780 nm, P = 375 mW cm^{-1}, irradiation time = 15 min.

MEH/light and CuS/MEH/light groups, respectively. These results indicated that after adding H_2O_2 into the group of CuS/MEH/light, the POD-like activity of CuS NPs was able to convert H_2O_2 into free radicals to induce more serious lipid peroxidation, further promoting the antibacterial activity of CuS NPs (Fig. 4c). Moreover, the fluorescent intensity of 2,7-Dichlorodihydrofluorescein diacetate (DCFH, a probe of reactive oxygen species) also increased obviously in CuS/H_2O_2/MEH/light (Fig. 4d), confirming the production of free radicals through POD-like catalytic reaction. The morphology and structural integrity of the bacteria treated by CuS/H_2O_2/MEH/light were also severely affected (Fig. S15†). Thus, visible-light irradiation was able to activate the antibacterial activity of the CuS/H_2O_2 system in the presence of a photoacid (Fig. 4e). This antibacterial activity was mainly correlated with two factors: the released-Cu^{2+} and the free radicals produced by the POD-like activity of the CuS NPs. Importantly, these two capacities were both pH dependent and could be simultaneously activated by visible light in the presence of a photoacid. In previous reports,[19,26] CuS NPs exhibited significant antibacterial activity due to their photothermal conversion performance. In our experiments, we demonstrated that CuS NPs could also showed the excellent antibacterial capability through exerting their enzyme mimicking activity. Although these two antibacterial modes were different, the results showed that CuS NPs could be applied as a potential antibacterial agent.

We next used an injury-infection model to further evaluate the antibacterial ability of our visible light-activated CuS nanozymes. As shown in Fig. 5a, each mouse exhibited marked weight loss after *S. aureus* infection for 24 h, indicating that the wound tissue was seriously infected. After treatment, we found that, compared with the control and other groups (Fig. 5b, c, and S16†), the CuS/H_2O_2/MEH/light group facilitated wound healing, whereas treatment with either CuS/MEH/light or H_2O_2 alone only induced moderate reduction in wound area. The wound closure rates on day 11 were 42.6%, 56.0%, and 88.1% for the H_2O_2, CuS/MEH/light, and CuS/H_2O_2/MEH/light-treated groups, respectively. The differences in the degrees of wound healing in the CuS/MEH and CuS/H_2O_2/MEH groups with and without light irradiation also indicated the importance of pH decrease induced by light illumination in the wound sites. Upon visible light illumination, a proton was rapidly produced through the intramolecular photoreaction of MEH, causing pH decrease in bacteria-infected wound sites, which activated the POD-like activity of CuS NPs to produce high levels of free

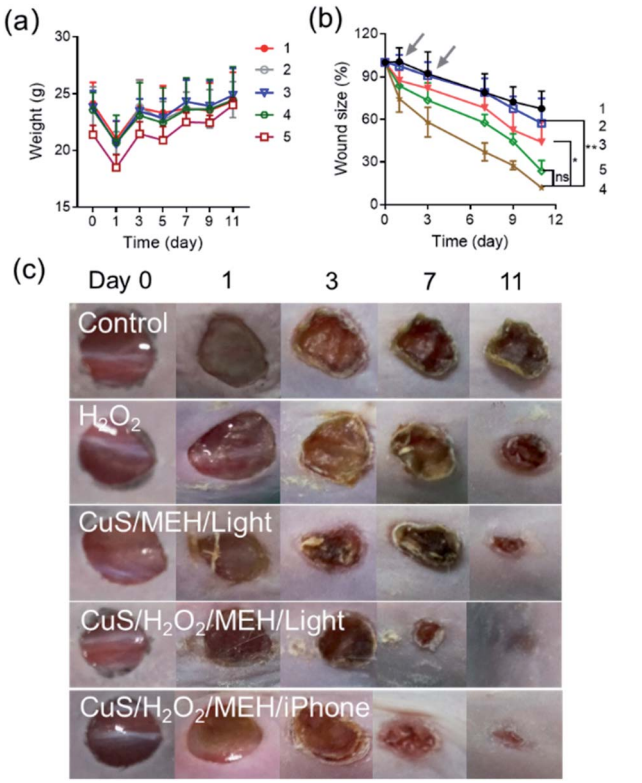

Fig. 5 Changes over time in (a) body weight and (b) wound area achieved in mice under different treatments. (1) Control; (2) H_2O_2; (3) CuS/MEH/light; (4) CuS/H_2O_2/MEH/light; (5) CuS/H_2O_2/MEH/iPhone. Arrow represents the time of administration. (c) Photographic images of wound healing degree in different groups. [MEH] = 500 μM; [CuS] = 500 μg mL^{-1}; [H_2O_2] = 10.0 mM. Illumination conditions: λ = 350–780 nm, P = 375 mW cm^{-1}, irradiation time = 15 min. For the iPhone group, the distance between light source and tested samples was 1 cm, and the illumination time was 15 min.

radicals, thus facilitating for killing bacteria and accelerating wound healing. Moreover, the pH decrease could trigger the Cu^{2+} release from CuS NPs, which further promoted the antibacterial performance. Notably, when we used the built-in torch of an iPhone to replace the visible light, a satisfactory outcome in wound healing was achieved, with a wound closure rate of 76.4% on day 11 (Fig. 5c). Together, these results demonstrated the effectiveness of a light-activated peroxidase mimic, in combination with released Cu^{2+}, reducing the burden of bacterial infections *in vivo*.

Conclusions

In summary, we developed a simple platform to activate the biomimetic activity of CuS NPs to kill bacteria. Considering that the POD-like activity of CuS NPs was pH-dependent and was deactivated easily in the bacteria-infected wounds. Thus, we introduced a photoacid into the system of CuS/H_2O_2. Upon light irradiation, the intramolecular photoreaction of MEH induced the pH decrease in wound sites, thus activating the activity of CuS NPs to produce high levels of free radicals, finally facilitating for killing bacteria and accelerating wound healing. Moreover, the pH decrease could also trigger the Cu^{2+} release from CuS NPs, which further promoted the antibacterial performance. Importantly, the built-in torches of mobile phones were able to replace the visible-light source, which greatly promotes the utility and adaptability of this antibacterial platform.

Conflicts of interest

There are no conflicts to declare.

Acknowledgements

This project was funded by the National Natural Science Foundation of China (No. 21703198). The authors also gratefully acknowledge financial support from the Priority Academic Program Development of Jiangsu Higher Education Institutions and Top-notch Academic Programs Project of Jiangsu Higher Education Institutions.

Notes and references

1 D. Jiang, D. Ni, Z. T. Rosenkrans, P. Huang, X. Yan and W. Cai, *Chem. Soc. Rev.*, 2019, **48**, 3683–3704.
2 Y. Huang, J. Ren and X. Qu, *Chem. Rev.*, 2019, **119**, 4357–4412.
3 X. Wang, L. Qin, M. Zhou, Z. Lou and H. Wei, *Anal. Chem.*, 2018, **90**, 11696–11702.
4 J. Wu, X. Wang, Q. Wang, Z. Lou, S. Li, Y. Zhu, L. Qin and H. Wei, *Chem. Soc. Rev.*, 2019, **48**, 1004–1076.
5 K. Korschelt, M. N. Tahir and W. Tremel, *Chemistry*, 2018, **24**, 9703–9713.
6 Z. Wang, Y. Zhang, E. Ju, Z. Liu, F. Cao, Z. Chen, J. Ren and X. Qu, *Nat. Commun.*, 2018, **9**, 3334.
7 C. Wang, C. Liu, J. Luo, Y. Tian and N. Zhou, *Anal. Chim. Acta*, 2016, **936**, 75–82.
8 P. C. Naha, Y. Liu, G. Hwang, Y. Huang, S. Gubara, V. Jonnakuti, A. Simon-Soro, D. Kim, L. Gao, H. Koo and D. P. Cormode, *ACS Nano*, 2019, **13**, 4960–4971.
9 H. Sun, N. Gao, K. Dong, J. Ren and X. Qu, *ACS Nano*, 2014, **8**, 6202–6210.
10 H. Wang, K. Wan and X. Shi, *Adv. Mater.*, 2018, e1805368.
11 P. Mostafalu, A. Tamayol, R. Rahimi, M. Ochoa, A. Khalilpour, G. Kiaee, I. K. Yazdi, S. Bagherifard, M. R. Dokmeci, B. Ziaie, S. R. Sonkusale and A. Khademhosseini, *Small*, 2018, e1703509.
12 R. Li, T. Nakashima, R. Kanazawa, O. Galangau and T. Kawai, *Chem.–Eur. J.*, 2016, **22**, 16250–16257.
13 W. H. Zhou, K. L. Braun, T. Y. Yu, J. K. Cammack, C. K. Ober, J. W. Perry and S. R. Marder, *Science*, 2002, **296**, 1106–1109.
14 R. M. D. Nunes, M. Pineiro and L. G. Arnaut, *J. Am. Chem. Soc.*, 2009, **131**, 9456–9462.
15 Z. Shi, P. Peng, D. Strohecker and Y. Liao, *J. Am. Chem. Soc.*, 2011, **133**, 14699–14703.
16 H. Lee, S. W. Yoon, E. J. Kim and J. Park, *Nano Lett.*, 2007, **7**, 778–784.
17 S. Goel, F. Chen and W. Cai, *Small*, 2014, **10**, 631–645.
18 J. Huang, J. Zhou, J. Zhuang, H. Gao, D. Huang, L. Wang, W. Wu, Q. Li, D. P. Yang and M. Y. Han, *ACS Appl. Mater. Interfaces*, 2017, **9**, 36606–36614.
19 Y. Qiao, Y. Ping, H. Zhang, B. Zhou, F. Liu, Y. Yu, T. Xie, W. Li, D. Zhong, Y. Zhang, K. Yao, H. A. Santos and M. Zhou, *ACS Appl. Mater. Interfaces*, 2019, **11**, 3809–3822.
20 T. P. Mofokeng, M. J. Moloto, P. M. Shumbula and P. Tetyana, *Anal. Biochem.*, 2019, **580**, 36–41.
21 Q. Feng, Y. Xu, B. Hu, L. An, J. Lin, Q. Tian and S. Yang, *Chem. Commun.*, 2018, **54**, 10962–10965.
22 Y. Xu, J. Fei, G. Li, T. Yuan, Y. Li, C. Wang, X. Li and J. Li, *Angew. Chem., Int. Ed.*, 2017, **56**, 12903–12907.
23 L. Gao, J. Zhuang, L. Nie, J. Zhang, Y. Zhang, N. Gu, T. Wang, J. Feng, D. Yang, S. Perrett and X. Yan, *Nat. Nanotechnol.*, 2007, **2**, 577–583.
24 X. Li, W. L. Yang, H. J. He, S. H. Wu, Q. Zhou, C. P. Yang, G. M. Zeng, L. Luo and W. Lou, *Bioresour. Technol.*, 2018, **251**, 274–279.
25 Q. Zhou, X. Li, Y. Lin, C. P. Yang, W. C. Tang, S. H. Wu, D. H. Li and W. Lou, *Water Res.*, 2019, **158**, 171–181.
26 M. Li, X. Liu, L. Tan, Z. Cui, X. Yang, Z. Li, Y. Zheng, K. Yeung, P. K. Chue and S. Wu, *Biomater. Sci.*, 2018, **6**, 2110–2121.